Data Article

Pressure drop data of two-phase flow in a horizontal tube filled with metal sponge

Sonja WEISE, Sarah KLEIN, Thomas WETZEL, Benjamin DIETRICH

Karlsruhe Institute of Technology, Institute of Thermal Process Engineering (TVT), Kaiserstr. 12, Karlsruhe, Germany

Abstract

Experimental data on the adiabatic and diabatic two-phase flow of saturated CO_2 in a horizontal cylindrical tube (diameter 14 mm) with integrated metal sponges (open-cell metal foams) are presented. Moreover, the pressure drop of single-phase flow inside the same metal sponges was investigated. The nominal cell density of the sponges is 10 ppi ("pores per inch") or 20 ppi. The mass flow was varied from 25 kg m^{-2} s^{-1} to 150 kg m^{-2} s^{-1} and the flow vapor quality from 0.1 to 1 in case of two-phase flow. The saturation pressure was either 12 bar or 26.5 bar. The length filled with sponges upstream of the test section varied from 12 mm to 210 mm for 10 ppi sponges and was 109 mm for 20 ppi sponges. In addition, geometric properties of the sponges relevant to pressure loss, such as window diameter, strut diameter, porosity and specific surface area, were determined.

Experimentelle Daten zur Zweiphasenströmung von gesättigtem CO_2 in einem horizontalen zylindrischen Rohr (Durchmesser 14 mm) mit integrierten Metallschwämmen (offenzellige Metallschäume) unter adiabaten sowie diabaten Bedingungen werden vorgestellt. Außerdem wurde der Druckverlust bei einphasiger Durchströmung derselben Schwämme untersucht. Die nominelle Zelldichte der Schwämme beträgt 10 ppi („Poren pro Zoll") bzw. 20 ppi. Der Massenstrom wurde von 25 kg m^{-2} s^{-1} bis 150 kg m^{-2} s^{-1} variiert und im Falle einer Zweiphasenströmung ebenfalls der Strömungsdampfgehalt (von 0,1 bis 1). Der Sättigungsdruck betrug entweder 12 bar oder 26,5 bar. Die mit Schwämmen gefüllte Länge stromaufwärts der Messstrecke variierte zwischen 12 mm und 210 mm bei 10 ppi Schwämmen und betrug 109 mm bei 20 ppi Schwämmen. Zusätzlich wurden die für den Druckverlust relevanten geometrische Eigenschaften der Schwämme, nämlich der Fensterdurchmesser, der Stegdurchmesser, die Porosität und die spezifische Oberfläche, bestimmt.

Contact: benjamin.dietrich@kit.edu; thomas.wetzel@kit.edu

Specifications Table

Subject area	Engineering, two-phase fluid flow through porous media
Type of data	Excel table
How data was acquired	Flow boiling test facility at the Institute of Thermal Process Engineering, Karlsruhe Institute of Technology
Data format	Analyzed
Experimental factors	<u>Sponges</u> 10 ppi copper sponge (total length 200 mm, diameter 14 mm) made by replication technique • total porosity: 91% • open porosity: between 85% and 88% • nominal cell density: approximately 10 pores per inch • mean strut diameter: 0.45 mm • mean window diameter: 1.6 mm 10 ppi plastic sponge (total length 47 mm, diameter 14 mm) made by 3D printing • total and open porosity: 86% • nominal cell density: approximately 10 pores per inch • mean strut diameter: 0.6 mm • mean window diameter: 2.0 mm 20 ppi copper sponge (total length 247 mm, diameter 14 mm) made by replication technique • total porosity: 90% • open porosity: between 84% and 87% • nominal cell size: approximately 20 pores per inch • mean strut diameter: 0.28 mm • mean window diameter: 1.0 mm <u>Operating conditions</u> • two-phase flow: pressure: 12 bar and 26.5 bar mass flux: 25 kg m^{-2} s^{-1} to 150 kg m^{-2} s^{-1} vapor quality: 10% to 100% o adiabatic: heat flux: less than 0.9 kW m^{-2} o diabatic: heat flux: 8 kW m^{-2} to 40 kW m^{-2} • single-phase flow: temperature: -10 °C to -15 °C mass flux: 25 kg m^{-2} s^{-1} to 150 kg m^{-2} s^{-1} heat flux: less than 0.9 kW m^{-2}

Data sets

sponge type	measurment type		pressure /bar	length upstream / mm
10 ppi	single-phase	diabatic		12
10 ppi	two-phase	adiabatic	12	12
10 ppi	two-phase	adiabatic	26.5	12
10 ppi	two-phase	adiabatic	26.5	210
20 ppi	single-phase	adiabatic/diabatic		109
20 ppi	two-phase	adiabatic	12	109
20 ppi	two-phase	adiabatic	26.5	109
20 ppi	two-phase	diabatic	12	109
20 ppi	two-phase	diabatic	26.5	109

Experimental features	Flow boiling test facility with test section (horizontal tube, diameter 14 mm, distance between pressure taps: 247 mm) especially designed to observe the heat transfer coefficient, the pressure drop and the flow pattern at a specific mass flux, vapor quality, saturation pressure, and heat flux
Data source location	Repository KITopen
Related research article	S. Weise, S. Meinicke, T. Wetzel, B. Dietrich, Modelling the pressure drop of two-phase flow through solid porous media, Journal of Multiphase Flow, submitted (2018).

Value of the Data

- data can be used to validate models describing the two-phase pressure drop in consolidated porous media, i.e. sponges
- data can be used to derive the influence of geometrical properties of the sponges
- data can be used to assess the efficiency of integrating metal sponges into horizontal evaporator tubes for enhancing flow boiling processes

Data

Data of adiabatic two-phase pressure drop of carbon dioxide (CO_2, R744) flowing through a copper sponge featuring a total porosity of 91% and an approximate cell density of 10 ppi ("pores per inch"), integrated into a horizontal tube with a diameter of 14 mm, is presented. The 10 ppi copper sponge covered 81% of the length between the pressure taps, the rest was filled with a similar plastic sponge. Moreover, data of adiabatic and diabatic two-phase pressure drop of carbon dioxide flowing through a copper sponge with a total porosity of 90% and an approximate cell density of 20 ppi integrated into the same horizontal tube with a diameter of 14 mm is presented. The 20 ppi copper sponge covered the total length between the pressure taps. For both sponge types, single-phase pressure drop data is provided additionally for selected operating conditions.

The mass flux, $\dot{m}$, vapor quality, $\dot{x}$, saturation pressure, p, of each data point is specified. In case of diabatic pressure drop, the heat flux, $\dot{q}$, related to the area between the pressure taps, is presented as well. The temperature of the liquid at the middle of the test section, T_{mean}, is provided for single phase data. The extended measurement uncertainty (coverage factor k=2), 2σ, and the standard deviation of 40 subsequent data points, s, are reported. All pressure drop measurements presented in this paper were carried out at the flow boiling test facility of the Institute of Thermal Process Engineering (TVT) at KIT [1–5]. Two-phase experiments were conducted at saturation pressures of 12 bar and 26.5 bar (corresponding to a saturation temperature of -35 °C and -10 °C, respectively), a mass flux between 25 kg m^{-2} s^{-1} and 150 kg m^{-2} s^{-1}, a vapor quality of 10% to 100%. The heat flux is less than 0.9 kW m^{-2} for near-adiabatic experiments. This corresponds to a change in vapor quality of less than 0.4%.

Experimental Design, Materials, and Methods

Test facility

A process flow diagram of the TVT flow boiling test facility is shown in Fig. 1. Pure CO_2 (purity grade 4.5), stored in a tank, is subcooled and pumped into the test loop. The mass flow rate of the subcooled liquid is measured by a Coriolis mass flow meter (Promass F 60 by Endress + Hauser) and adjusted with an electronic control valve. The vapor quality in the middle of the test section is adjusted by three pre-heaters in series according to an enthalpy balance. The last pre-heater upstream of the test section is a smooth tube with the same inner diameter as the test section. Downstream of the test section, a sight glass is installed to enable the observation of flow patterns.

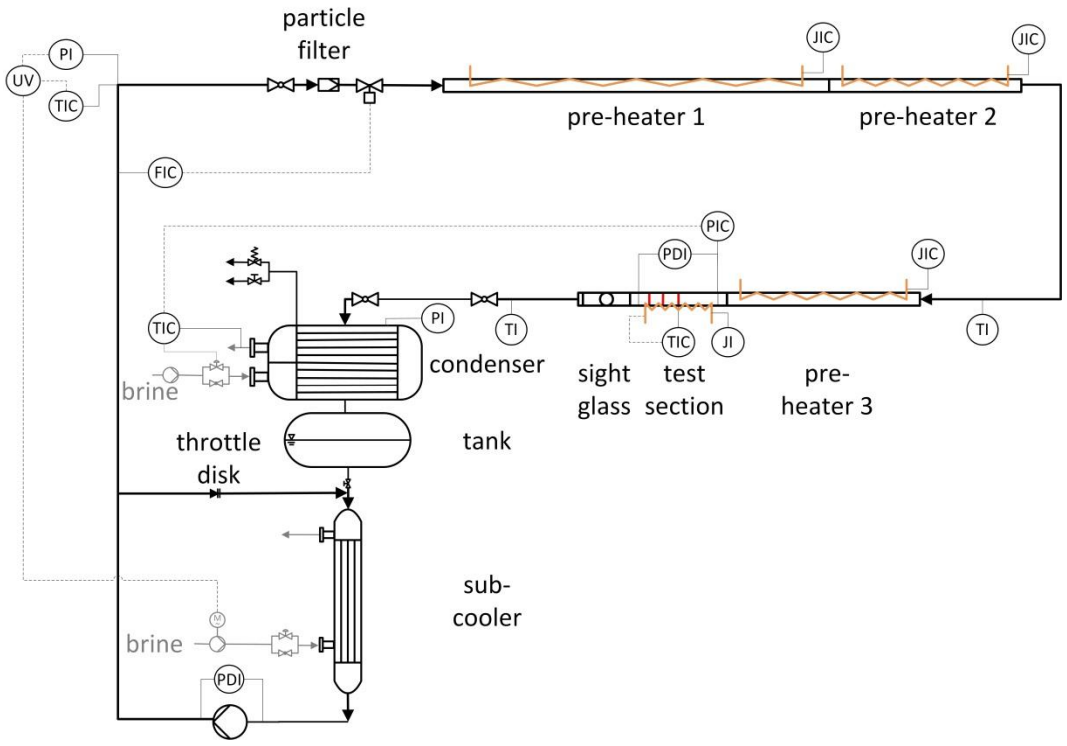

Fig. 1.
Process flow diagram of the flow boiling test facility.

During adiabatic measurements, the test section is not heated. The heat flux through the insulation is less than 0.6 kW m^{-2} at 26.5 bar and less than 0.9 kW m^{-2} at 12 bar. For diabatic measurements, the test section is electrically heated over a length of 200 mm. The inlet pressure and the total static pressure drop are measured and recorded in steady state. Each reported data point represents an average of 40 data points recorded within 50 s. Downstream of the test section and the sight glass, the vapor is re-liquefied in the condenser. Steady state is ensured by a start-up period of 40 minutes and a waiting time of at least 3 minutes after small changes until all parameters are constant within a specified range within three minutes ($\Delta\dot{m} < 1$ kg m^{-2} s^{-1}, $\Delta p < 0.02$ MPa, $\Delta\dot{x} < 0.01$, $\Delta\Delta p < 1$ mbar (10 ppi) or < 7 mbar (20 ppi)). The standard deviation of the 40 data points is less than $s(\dot{m}) < 0.8$ kg m^{-2} s^{-1}, $s(p) < 0.002$ MPa, and $s(\Delta p) < 0.4$ mbar for the 10 ppi sponge and $s(\dot{m}) < 3$ kg m^{-2} s^{-1} and $s(\Delta p) < 11$ mbar for $p = 12$ bar, and $\dot{m} > 100$ kg m^{-2} s^{-1} for the 20 ppi sponge. To check the validity of these preset conditions, each recording is repeated after 5 minutes.

Test section

In Fig. 2, an axial view of the test section and the sight glass directly adjoining the test section is depicted. The test section is made of a brass tube with an inner diameter of 14.00 mm $\pm$0.01 mm and a mean arithmetic surface roughness of $R_A = 0.8 \cdot 10^{-6}$ m. Six holes were drilled around the circumference at both the inlet and the outlet of the tube to connect the tube to two annular chambers integrated in inlet and outlet flange. The annular chamber ensures the correct measurement of an average static pressure of the two-phase flow, irrespective of the flow pattern. The inlet pressure tap is connected to a pressure transducer (Burster 8103-50). Inlet and outlet pressure taps are connected to a differential pressure transducer (Rosemount 3051C) measuring the pressure difference at a distance of $L = 247$ mm.

The copper sponge to be examined was inserted into the test section, see Fig. 2 for 10 ppi sponge and Fig. 3 for 20 ppi sponge, with a clearance fit of <70 µm. Due to manufacturing constraints, the sponge is composed of several short pieces. The copper sponge is framed by a plastic sponge in case of the 10 ppi sponge. The plastic sponge is inserted into the sight glass and the rest of the test section to prevent axial heat flux out of the heated zone. A coarse sieve adjoining the sight glass provides fixation of the sponge. The total length of the 10 ppi copper sponge samples between the pressure taps, L_{Cu}, is 200.2 mm. This corresponds approximately to the heated length (200 mm). The sample diameter of the copper sponge, measured by a micrometer screw gauge with an extended measurement uncertainty of ±0.05 mm, is $13.96\ ^{+0.02}_{-0.03}$ mm (10 ppi) or $13.97\ ^{+0.02}_{-0.02}$ mm (20 ppi). The length filled with plastic sponge upstream of the inlet pressure tap, L_e, was varied from 12 mm to 210 mm (10 ppi) or equals 109 mm (20 ppi).

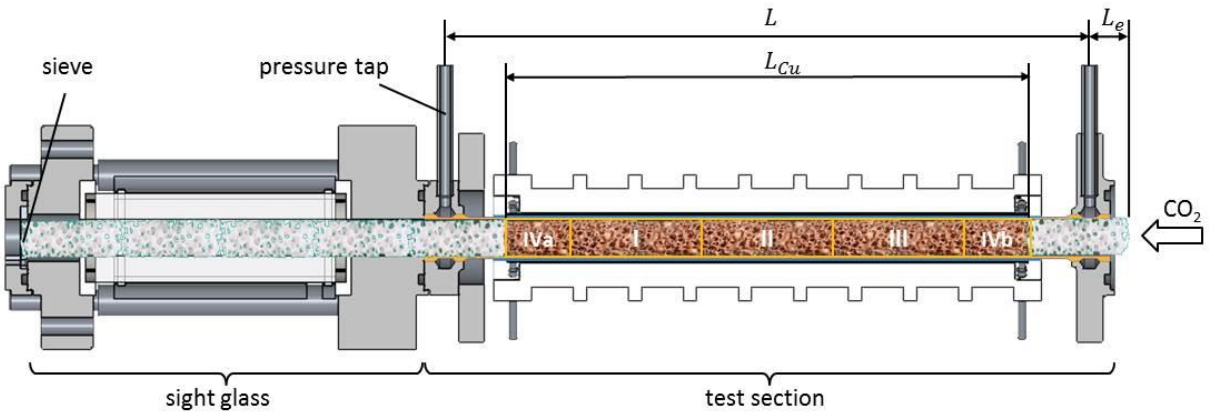

Fig. 2.
Axial view of the test section and sight glass filled with 10 ppi copper and plastic sponge. Relevant lengths are the distance between the pressure taps, L, and the total length of the copper sponge samples, L_{Cu}, which equals the heated length.

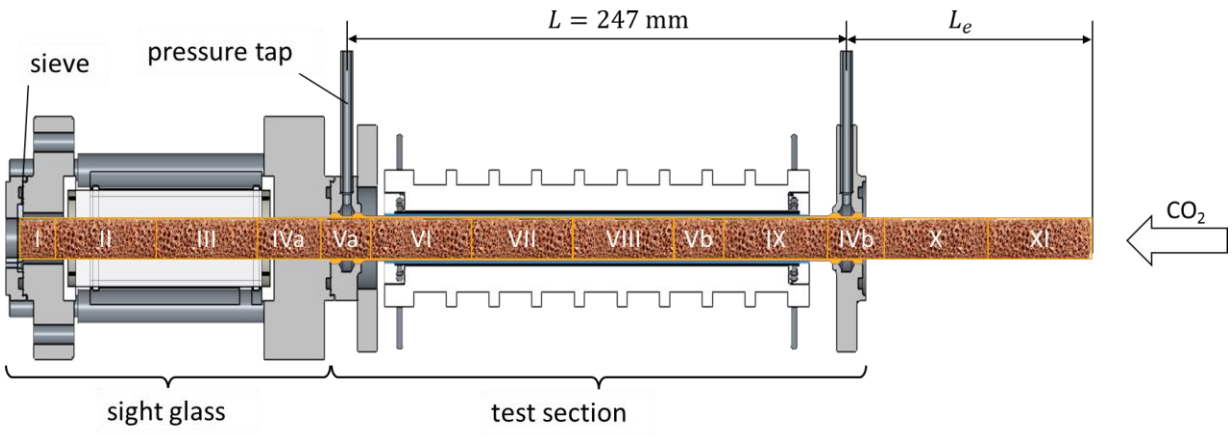

Fig. 3.
Axial view of the test section and sight glass filled with 20 ppi copper sponge. Relevant lengths are the distance between the pressure taps, L.

Data reduction and measurement uncertainty

The mass flux, $\dot{m}$, is related to the cross-sectional area of the empty tube. The mean vapor quality (in the center of the test section) is calculated by means of an enthalpy balance between the entrance of the test conduit, at which the refrigerant is subcooled, and the middle of the test section assuming thermodynamic equilibrium. Parasitic heat transfer from the environment through the insulation as well as the power supplied by the preheaters is taken into account. The heat transfer from the environment is estimated by means of the thermal transmittance, which is determined at vacuum conditions and validated by single-phase measurements. The pressure drop per unit length equals the measured pressure drop, Δp^*, divided by the distance between the pressure taps, L. For single phase measurements, the liquid temperature at the center of the test section is calculated by means of an enthalpy balance based on the temperature before pre-heater 3. In case of diabatic experiments, the heat flux is calculated by dividing the total heat transfer to the test section (electric heating and parasitic heat transfer) by the tube's inner surface area between the pressure taps.

For each measuring instrument, either the extended measurement uncertainty according to the "Guide to the expression of uncertainty in measurement" (GUM) [6] with a coverage factor of k=2 describing a confidence level of 95%, or specifications given by the manufacturer are listed in Table 1. The GUM analysis was described in detail by Wetzel et al. [3] for resistance thermometers and pressure transducers.

Table 1.
Extended instrument uncertainties and manufacturer specifications.

mass flow meter	±0.15% of reading; ±0.02% of range[a]
digital power meter	±0.2% of reading; ±0.1% of range[a]
pressure transducer	±0.025 bar[b]
resistance thermometer (PT100)	±0.023 K[b]
differential pressure transducer (URV = 20 mbar)	±0.3 mbar[b]
differential pressure transducer (URV = 500 mbar)	±0.7 mbar[b]

a) specification given by the manufacturer. b) result of extended uncertainty analysis (k=2).

The GUM analysis was further applied to derive the extended measurement uncertainty for all reported quantities on a basis of the extended measurement uncertainty of the respective devices, whereby the uncertainty of any auxiliary procedure like calibration was taken into account. The extended measurement uncertainty (k=2), 2σ, is given for each data point.

The reproducibility of pressure drop of a tube filled with sponge was demonstrated by comparing data recorded by different persons on different days at intervals of several weeks. These data coincide within the scope of the measurement uncertainty.

Sponges

The investigated copper sponges were obtained from the Fraunhofer Institute for Manufacturing Technology and Advanced Materials (IFAM) in Dresden (compare Fig. 4). Several blocks were made by replication technique [7] using a polyurethane template.

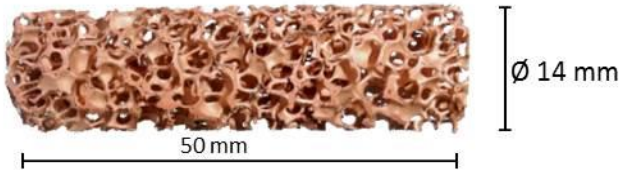

Fig. 4.
Photograph of one of the copper sponge samples (10 ppi), which were integrated in test section.

Table 2 and Table 3 provide an overview of averaged properties, their uncertainty and variation, as well as the methods for characterizing the copper samples used. The total porosity was determined for each sample. The strut diameter was measured halfway between two nodes, corresponding to the thinnest diameter of the strut. The window diameter was determined by averaging the major and minor axis, as the windows are ellipsoidal and feature a ratio of major to minor axis of approximately 1.5.

Table 2.

Geometric characteristics of the 10 ppi copper sponge samples integrated into the test section. Values are averaged for the samples. The maximum deviation between any sample's property and its mean value is given to assess their homogeneity. If not specified otherwise [(+)], the measurement uncertainty (k=2) according to GUM [6] of each method is given. Standard deviation of multiple measurements of the same structure, s, and standard deviation of the mean s_x, are given if applicable.

property	averaged value and maximum deviation	method/instrument	uncertainty of method (k=2)
nominal cell density	10 ppi	customary designation of template provider	-
total porosity, Ψ_t	sample I-IV: $90.7\ ^{+0.4}_{-0.3}$ %	direct method density of pure copper: 8.94 kg m^{-3} [8]	$2\sigma = \pm 0.07\%$
	sample V: 90.7%		
open porosity, Ψ_o	$87.6\ ^{+0.2}_{-0.2}$ %	gas pycnometry @ CVT, KIT (AccuPyc Pycnometer 1330)	$2\sigma = \pm 0.41\%$
	sample V: 85.5%	reconstruction of µCT scan (ZEISS Xradia 520 Versa, resolution 15 µm, test specimen: $h = 50$ mm; $d = 14$ mm)	
secondary porosity ($V_{\text{secondary pores}}/V_s$)	8.4%	digital image processing of light optical micrographs of metallographic specimen	$2\sigma = \pm 3.4\%$
mean strut diameter, d_s	sample I-III: 450 µm	optical microscope	$s_x = 16$ µm; $s = 103$ µm
	sample IV, V: 429 µm		$s_x = 24$ µm; $s = 132$ µm
mean window diameter, d_w	sample I-III: 1561 µm	optical microscope	$s_x = 63$ µm; $s = 332$ µm
	sample IV, V: 1580 µm		$s_x = 75$ µm; $s = 396$ µm
specific surface area, $S_v = \frac{A}{V_{cylinder}}$	sample V: 952 m^{-1}	reconstruction of µCT scan (ZEISS Xradia 520 Versa, resolution 15 µm, test specimen: h = 50 mm; d = 14 mm)	

Table 3.
Geometric characteristics of the 20 ppi copper sponge samples integrated into the test section. Values are averaged for the samples. The maximum deviation between any sample's property and its mean value is given to assess their homogeneity. If not specified otherwise [(+)], the measurement uncertainty (k=2) according to GUM [6] of each method is given. Standard deviation of multiple measurements of the same structure, s, and standard deviation of the mean s_x, are given if applicable.

property	averaged value and maximum deviation	method/instrument	uncertainty of method (k=2)
nominal cell density	20 ppi	customary designation of template provider	-
total porosity, Ψ_t	sample I-VII: $89.7\ ^{+0.8}_{-0.4}$ %		$2\sigma = \pm 0.07\%$
	sample VIII: 89.9%		
open porosity, Ψ_o	sample VIII: 86.8%	gas pycnometry @ CVT, KIT (AccuPyc Pycnometer 1330)	$2\sigma = \pm 0.41\%$
	sample VIII: 84.5%	reconstruction of µCT scan (ZEISS Xradia 520 Versa, resolution 15 µm, test specimen: $h = 50$ mm; $d = 14$ mm)	
secondary porosity ($V_{\text{secondary pores}}/V_s$)	8.4%	digital image processing of light optical micrographs of metallographic specimen	$2\sigma = \pm 3.4\%$
mean strut diameter, d_s	sample II-IV,X: 246 µm	optical microscope	$s_x = 10$ µm; $s = 56$ µm
	sample VI-VIII: 275 µm		$s_x = 14$ µm; $s = 72$ µm
mean window diameter, d_w	sample II-IV,X: 1130 µm	optical microscope	$s_x = 58$ µm; $s = 273$ µm
	sample VI-VIII: 1027 µm		$s_x = 53$ µm; $s = 238$ µm
specific surface area, $S_v = \frac{A}{V_{cylinder}}$	sample X: 1375 m^{-1}	reconstruction of µCT scan (ZEISS Xradia 520 Versa, resolution 15 µm, test specimen: h = 50 mm; d = 14 mm)	

Table 4 provides an overview of averaged properties of the plastic sponge made of VisiJet® M2-RCL, an acrylate polymer, 3D printed by KSP GmbH. This sponge were inserted upstream and downstream of the 10 ppi copper sponge samples. The length of the plastic sponge amounts to 18.9% of the distance between the pressure taps. At the time of 3D printing of the plastic sponges, no µCT scan of the copper sponge was available. Hence, a µCT scan of a 10 ppi ceramic sponge was used to create the 3D model for printing the plastic sponge. The geometric properties of this ceramic sponge are comparable to those of the copper sponge. This 3D model first had to be edited manually to ensure printability, i.e. internal pores were closed with CAD software and artefacts were cleaned up. The geometric properties of the plastic sponge, listed in Table 4 were derived from this 3D CAD model and checked with the optical microscope after use in the test section. The struts seem to be slightly thicker than specified by the 3D CAD model. The real macroscopic surface area therefore probably deviates slightly from the macroscopic surface area determined from the 3D CAD model.

Table 4.
Geometric characteristics of the plastic sponge samples integrated into the test section. Values are derived from 3D CAD model and compared to values obtained by optical microscopy (*). Standard deviation, s, and standard deviation of the mean, s_x, are given if applicable.

property	averaged value	comment
total porosity, $\Psi_t\ (=\Psi_0)$	85.5%	
mean strut diameter, d_s	580 µm	s_x= 20 µm s = 142 µm
	650 µm (*)	s_x= 18 µm (*) s = 87 µm (*)
mean window diameter, d_w	2380 µm	s_x= 154 µm s = 598 µm
	2000 µm (*)	s_x= 117 µm (*) s = 523 µm (*)
macroscopic surface area, $S_{v,\mathrm{incl}}$	579.7 m^{-1}	including the fraction of the cylinder shell surface covered by the porous structure, voxel size of underlying µCT-scans: 0.056 mm, coarsened with triangulation length: 0.13 mm
macroscopic surface area, $S_{v,\mathrm{excl}}$	530.1 m^{-1}	excluding surface area of intersection with cylinder $S_{v,\mathrm{excl}} = \frac{A_{\mathrm{incl}} - \Psi_t \cdot A_{\mathrm{cylinder}}}{V_{\mathrm{cylinder}}}$
sample diameter	13.9 mm	
sample length	36.6 mm	

Acknowledgments

The authors would like to thank the Deutsche Forschungsgemeinschaft for their financial support. Furthermore, we acknowledge the support of the Institute of Chemical Process Engineering (CVT), KIT for porosity measurements (gas pyconometry) and of the Institute for Applied Materials – Materials for Electrical and Electronic Engineering (IAM-WET), KIT for computed tomography scans. We further acknowledge the contribution of Anna-Maria Eckel, who characterized the geometry of the copper sponges.

Funding

This work was supported by the Deutsche Forschungsgemeinschaft
[grant number WE 4672/2-1].

References

[1] A.E. Schael, M. Kind, Flow pattern and heat transfer characteristics during flow boiling of CO_2 in a horizontal micro fin tube and comparison with smooth tube data, Int. J. Refrig. 28 (2005) 1186–1195.

[2] A.E. Schael, Über das Strömungsverdampfen von CO_2 im glatten und innen berippten Rohr - Hydrodynamik, Wärmeübergang, Druckverlust, Ph.D. Thesis, Universität Fridericiana Karlsruhe (TH), Karlsruhe, 2009.

[3] M. Wetzel, B. Dietrich, T. Wetzel, Influence of oil on heat transfer and pressure drop during flow boiling of CO_2 at low temperatures, Exp. Therm. Fluid Sci. 59 (2014) 202–212.

[4] M. Wetzel, Influence of fully miscible lubrication oil on flow boiling of CO_2 inside horizontal evaporator tubes, Ph.D. Thesis, Karlsruher Institut für Technologie, Karlsruhe, 2017.

[5] S. Weise, M. Wetzel, B. Dietrich, T. Wetzel, Influence of fully miscible lubricating oil on the pressure drop during flow boiling of CO_2 inside an enhanced tube, Exp. Therm. Fluid Sci. 81 (2017) 223–233.

[6] International Organization for Standardization, Guide to the expression of uncertainty in measurement (GUM), 1993.

[7] P. Quadbeck, K. Kümmel, R. Hauser, G. Standke, J. Adler, G. Stephani, Open Cell Metal Foams – Application-oriented Structure and Material Selection, in: Proc. of CellMAT, 2010.

[8] Deutsches Kupfer-Institut, DKI Werkstoff-Datenblätter, 2005.